CHINA FOUNDRY Research & Development
Vol. 23 No. 6 November 2026
www.springer.com/41230
https://doi.org/10.1007/s41230-026-4269-4

Microstructure and mechanical properties of fine-grained K417 superalloy ring fabricated by vacuum centrifugal casting

Xiao-qing Ma[1], Min-le Liao[1], Chi Zhang[2], *Guo-huai Liu[1], and **Zhao-dong Wang[1, 3]

1. State Key Laboratory of Rolling and Automation, Northeastern University, Shenyang 110819, China

2. School of Materials Science and Engineering, Shenyang University of Technology, Shenyang 110870, China

3. Institute of Materials, Henan Academy of Sciences, Zhengzhou 450046, China

Copyright © 2026 Foundry Journal Agency

Abstract: The K417 superalloy rings are extensively applied in the aerospace field for its excellent high-temperature strength and outstanding high-temperature creep resistance. However, conventional manufacturing routes face challenges in complex processing procedures and low material utilization. This work presents a vacuum centrifugal casting process to directly fabricate fine-grained K417 ring. Numerical simulation of grain structure established the correlation between processing parameters and microstructural development. Using the optimized processing parameters, the prepared K417 ring exhibits a fine grain structure (ASTM 4) with minimal porosity (below Grade one). No macrosegregation is observed with homogeneous element distribution throughout the ring. The γ' phase is uniformly distributed in the matrix as the main strengthening phase, accompanied by γ/γ' eutectic phases and MC carbides precipitated at the grain boundaries. The tensile strength is 1,115.3 MPa at 20 °C, 725 MPa at 900 °C, and 409.6 MPa at 1,000 °C, with elongation of 10.4%, 8.5%, and 9.1%, respectively. Microstructural analysis indicates that cracks mainly originate near MC carbides and eutectic phases. As the tensile temperature increases from 20 °C to 1,000 °C, the fracture form gradually transitions from transgranular to intergranular fracture.

Keywords: K417 superalloy; vacuum centrifugal casting; microstructure; tensile

CLC numbers: TG146.1+5 **Document code:** A **Article ID:** 1672-6421(2026)06-794-13

1 Introduction

The nickel-based K417 superalloy is widely used in aeroengine components such as turbine disks, turbine blades, and gas turbines for its low density, good high-temperature strength, creep resistance, and oxidation resistance[1-3]. The K417 superalloy rings, as key components, are used in bearing races, casings, combustion chambers, and sealing rings, etc[4, 5]. However, the conventional preparation process of rings is complicated, involving blank opening, initial forging, blanking, upsetting, and punching. The process is complex, where the material utilization rate is low and the preparation cost is high[6]. In order to solve the above problems, researchers have carried out much related research work in the field of short process, low cost, and green preparation of rings[7-9]. However, the forming process of rings involves many complex phenomena such as crystallization, grain growth, solute diffusion, inclusions, etc, so it is difficult to prepare rings that meet the requirements[10-12].

The advent of centrifugal casting process can, to some extent, resolve the aforementioned challenges with providing a short process to prepare high-quality rings directly. Firstly, this process has a unique periodic centrifugal force, which, in the production of symmetrical components, offers a distinct advantage. The rings can be directly prepared, therefore reducing the complexity of the process[13, 14]. Secondly, centrifugal casting differs from gravity casting in

***Guo-huai Liu**

Male, Ph. D., Associate Professor. His research interests mainly focus on Ni-based superalloys, Ti alloys, and TiAl alloys.

E-mail: liugh@ral.neu.edu.cn

****Zhao-dong Wang**

Male, Ph. D., Professor. His research interests mainly focus on the advanced rolling technology and heat treatment of metal materials.

E-mail: zhdwang@mail.neu.edu.cn

Received: 2024-12-23; Revised: 2025-01-23; Accepted: 2025-02-24

that it utilizes centrifugal force to obtain a casting with high density, fine grain, and uniform wall thickness, making it an effective method for producing high-quality components[15-17]. Additionally, the centrifugal force can accelerate the discharge of impurities from the melt, promoting the remelting of dendrite and the breakdown of grain boundary by flow field and vibration, and accelerating the growth of the crystalline core[18, 19]. Compared to gravity casting, the pouring process of centrifugal casting can be performed without risers, and it eliminates the need for cores, thereby saving raw materials, and enhancing the utilization efficiency of metals. In addition, it can also refine the grain structure and improve the performance of the materials[20, 21]. Centrifugal casting is a cost-effective and convenient method that has been widely applied in the production of metal materials and composite materials[22, 23]. Ma et al.[24] studied the microstructure and properties of Mg-9Li-3Al-1Ca alloy, finding that centrifugal casting can break the long strip structure in ordinary gravity casting, refine and spheroidize the long strip structure. Compared with gravity casting, centrifugal casting process can significantly improve the strength and elongation of Mg-9Li-3Al-1Ca alloy. Kang et al.[25] studied the effect of centrifugal casting on the properties of nickel-based superalloy thin-walled parts. Compared with conventional gravity casting, the results show that the centrifugal casting has fewer risers and exhibits fewer Laves harmful phases, leading to a significant improvement in the alloy's strength. Yang et al.[26], through simulation and experimental comparison, analyzed the density of parts prepared by gravity casting and centrifugal casting, discovering that centrifugal casting could significantly reduce the formation of porosity defects and improve material density. Vacuum centrifugal casting, as a type of centrifugal casting, could further prevent the formation of defects during casting, prevent the oxidation of alloys, maintain the stability of chemical composition, and promote the uniform crystallization and refinement through its high vacuum environment, thereby enhancing the final material's properties.

However, the centrifugal casting process involves complex alloy liquid flow and filling problems, and improper casting process parameters affect the filling and solidification of the alloy, potentially leading to grain growth and the change of precipitation phase morphology, all of which can impact the alloy's performance and its deformation mechanism. This shows that controlling the grain structure established during solidification is crucial to mechanical properties. At present, although many research works have been done to reveal the performance of K417 superalloy, there is still a lack of systematic research on K417 superalloy under the specific casting process of vacuum centrifugal casting. Therefore, based on the above situation, it is necessary to study the microstructure and mechanical properties of K417 superalloy by vacuum centrifugal casting. However, the solidification and forming process of the alloy under the action of the centrifugal force field is not transparent, and it requires a long cycle and high cost to rely solely on experimental exploration to determine the rationality of the centrifugal casting process parameters. Therefore, the use of casting simulation technology can not only help to shorten the experimental cycle, reduce cost, and minimize the risk of experimental trial and error, but also provide guidance for real pouring experiments by defining a reasonable range of pouring process parameters[27]. For example, Xin et al.[28] used the ProCAST simulation software to narrow down the pouring process parameter range for the 2060Al-Li alloy, and selected reasonable parameters for subsequent pouring experiments, saving preparation cost.

In this study, the K417 superalloy ring was taken as the main research object. The relationship between processing parameters and grain structure was established through numerical simulation, which determined the optimal pouring temperature and centrifugal speed. The K417 superalloy ring was then fabricated using these optimized parameters. This study focused on the microstructure, porosity defect distribution, segregation, and mechanical properties of the K417 superalloy ring. The tensile properties and fracture formation were discussed, and the internal mechanism was analyzed in depth. This study aims to evaluate the potential of vacuum centrifugal casting for producing high-performance K417 superalloy rings, offering insights into its application in aerospace components.

2 Simulation and experiment

2.1 Simulation

ProCAST software was used to simulate the centrifugal casting process of K417 superalloy. The optimal process parameters of centrifugal casting were determined according to the grain size and the proportion of equiaxed grain zone obtained under different process parameters. The specific simulation process is shown in Table 1. The three-dimensional model of the ring was drawn using UG software, and the mesh was divided using Promesh software. Mesh splitting units were integrated into the finite element mesh model for the castings, molds, and pouring system, employing tetrahedral mesh sizes of 3 mm, 10 mm, and 5 mm, respectively. The total number of meshes in the simulation amounted to approximately 830,000. The mesh size of the ring was set to be smaller than the mesh size of the mold, and the mesh division diagram is shown in Fig. 1. The gravity coefficient was set to 9.8 $m \cdot s^{-2}$, and the heat transfer coefficient was set to 5,000 $W \cdot m^{-2} \cdot K^{-1}$ due to the fast cooling rate of centrifugal casting. The casting mold was made using 45 steel, and air cooling was employed. The pouring temperatures were set at 1,380 °C, 1,420 °C, 1,500 °C, and 1,540 °C, with a rotation speed of 400 $r \cdot min^{-1}$. The rotational speeds were set to 200 $r \cdot min^{-1}$, 400 $r \cdot min^{-1}$, 600 $r \cdot min^{-1}$, and 800 $r \cdot min^{-1}$, while the pouring temperature was 1,460 °C. Several groups of processes with different pouring temperatures and centrifugal speeds were compared. The process conditions were set in the ProCAST software, and the material type of the alloy was set according to the chemical composition of the K417 superalloy. The thermal physical parameters of the K417 superalloy were calculated.

Table 1: ProCAST simulation process parameters

Process numbers	Centrifugal speeds ($r \cdot min^{-1}$)	Pouring temperatures (°C)	Process numbers	Centrifugal speeds ($r \cdot min^{-1}$)	Pouring temperatures (°C)
P1	200	1,460	P5	400	1,380
P2	400		P6		1,420
P3	600		P7		1,500
P4	800		P8		1,540

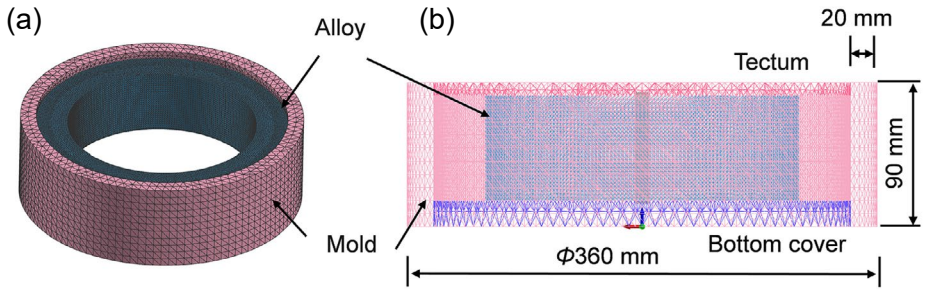


Fig. 1: Schematic diagram of grid division model for centrifugal casting: (a) mesh division model; (b) wireframe of centrifugal casting

2.2 Experiment

The K417 superalloy ring was prepared by centrifugal furnace according to the optimum process parameters simulated by ProCAST. The preparation process was as follows. The K417 superalloy cleaned by ultrasonic vibration was put into the Al_2O_3 crucible. Before melting, the rotary vane pump, rotary vane pump valve, rough pumping valve and pre-pumping valve were opened in turn to reduce the air pressure in the centrifugal furnace. When the pressure gauge showed 3,000 Pa, the Roots pump was opened to further reduce the furnace pressure until the vacuum reached below 10 Pa. Argon gas was repeatedly introduced for multiple furnace cleanings. The vacuum environment protected by argon can prevent the introduction of oxygen during the melting process to a large extent, which is beneficial for preparing excellent castings. The casting mold used a ring-shaped structural part made of AISI 1045 steel. The thermocouple was used for temperature measurement. After heating to 1,380 °C and holding for 5 min until the alloy was completely melted, the centrifugal speed of the equipment was set to 400 $r \cdot min^{-1}$. The molten metal was then poured uniformly and smoothly into the rotating mold, where the alloy liquid filled the mold under the action of centrifugal force and solidified into a cast ring. After the alloy liquid solidified and cooled, the mold was removed to obtain the ring with an outer diameter of 320 mm, an inner diameter of 260 mm, a wall thickness of 40 mm, and a height of 80 mm. The chemical composition of this ring, as measured by XPS, is shown in Table 2.

Table 2: Chemical composition (wt.%) of K417 superalloy measured by XPS

C	Cr	Co	Mo	Al	Ti	Fe	Ni
0.15	9.6	15.7	3.7	5.0	4.6	0.3	Bal.

The microstructure observation, element distribution measurement, grain size statistics, and mechanical properties testing of the ring were carried out. Cubic samples with dimensions of 10 mm×10 mm×5 mm were cut at different positions of the ring slice to observe grain structures and porosity defects. The porosity defects in the ring were observed after being mechanical ground and polished. Then, the microstructures were observed after being chemically etched using 1.5 g $CuSO_4$+40 mL HCl+20 mL C_2H_5OH by an Olympus GX 71 metallographic microscope. ImageJ software was used to measure the area proportion of porosity defects and γ' phase size. The evaluation of porosity grade refers to the micro-porosity evaluation method of HB+20058-2011 cast superalloy (specific requirements: the view field is enlarged by 100 times to take the area of microporosity after polishing the sample, and the ratio of the area of microporosity to the area of the view field was calculated). The morphology of precipitated phase of the ring by vacuum centrifugal casting was observed using a ZEISS ULTRA 55 field emission scanning electron microscope (SEM), and the grain size was measured by electron backscatter diffraction (EBSD). From the outer to inner ring, equal distances were selected, and energy-dispersive spectrometer (EDS) testing was performed at 10 different positions to analyze the overall compositional segregation of the sample. The tensile test was carried out on the WDW-300 electronic universal testing machine with a tensile rate of 1 $mm \cdot min^{-1}$. Tensile specimens at 20 °C, 900 °C, and 1,000 °C are shown in Fig. 2. The tensile fracture and the longitudinal section of the fracture were observed by SEM and EBSD to determine the crack source and fracture mechanism. The samples for EBSD were electrolytically polished in a solution of 10% $HClO_4$+90% C_2H_5OH for 22 s at a voltage of 20 V and a current of 1.67 A.

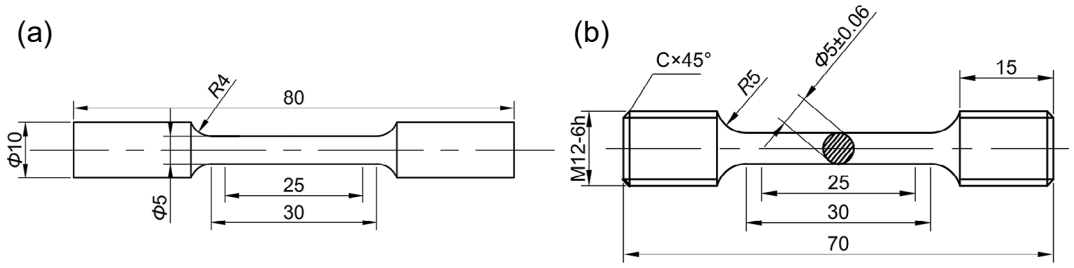


Fig. 2: Schematic diagram of tensile specimen at 20 °C (a), 900 °C and 1,000 °C (b) (unit: mm)

3 Results

3.1 Simulation results

Figures 3 and 4 show the solidification microstructures of the cast rings at different centrifugal speeds and pouring temperatures, respectively. The microstructures are composed of equiaxed grains and columnar grains. The proportion of columnar crystal area at different conditions was counted. At centrifugal speeds of 200 r·min^{-1}, 400 r·min^{-1}, 600 r·min^{-1}, and 800 r·min^{-1}, the columnar grain percentages are 65%, 30%, 40%, and 63%, respectively. Overall, there is a trend where the percentage of columnar grains firstly decreases and then increases with increasing centrifugal speed, while the percentage of equiaxed grains shows the opposite trend. At pouring temperatures of 1,380 °C, 1,420 °C, 1,500 °C, and 1,540 °C, the columnar grain percentages are 5%, 15%, 40%, and 55%, respectively. Overall, there is a trend where the percentage of columnar grains gradually increases with increasing pouring temperature, while the percentage of equiaxed grains gradually decreases. The average grain size at different pouring conditions is counted, as shown in Fig. 5. The results indicate that the change of centrifugal speed has no significant effect on the average grain size, which is generally concentrated around 207 μm. Additionally, with increasing pouring temperature, the grain size significantly increases from 186.24 μm at 1,380 °C to 229.89 μm at 1,540 °C, showing a marked influence of pouring temperature on grain size.

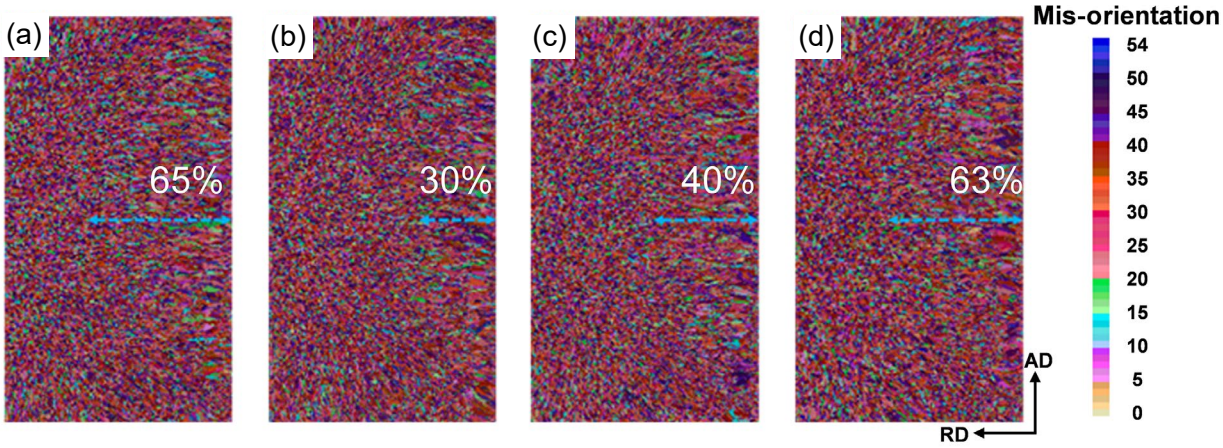


Fig. 3: Predicted microstructure under different centrifugal speeds and a pouring temperature of 1,460 °C: (a) 200 r·min^{-1}; (b) 400 r·min^{-1}; (c) 600 r·min^{-1}; (d) 800 r·min^{-1}

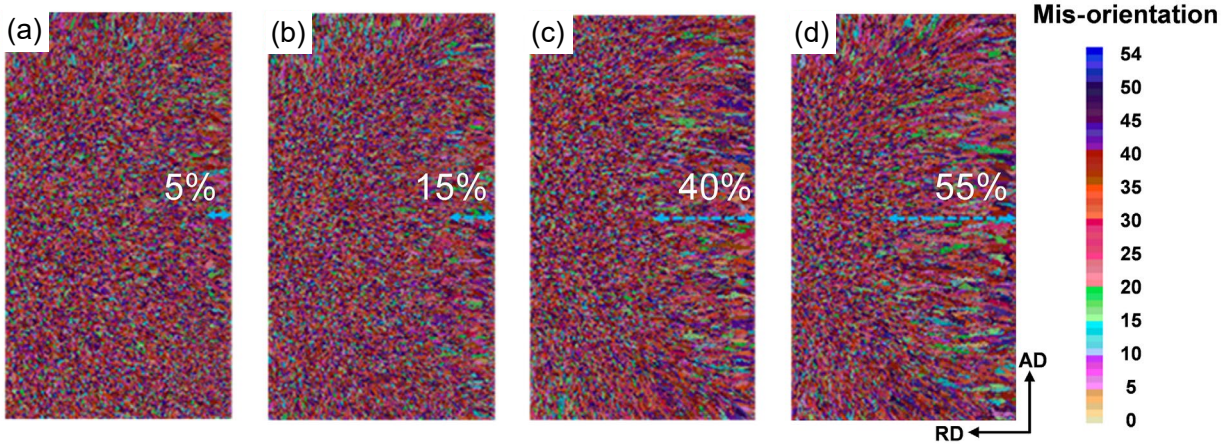


Fig. 4: Predicted microstructure under centrifugal speed of 400 r·min^{-1} and different pouring temperatures: (a) 1,380 °C; (b) 1,420 °C; (c) 1,500 °C; (d) 1,540 °C

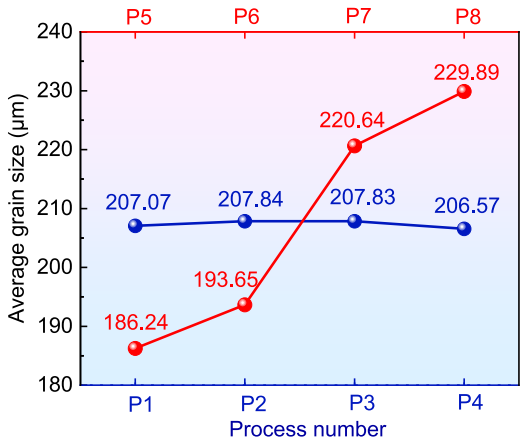


Fig. 5: Statistics of average grain size under different processes

According to the simulation results, it is found that the pouring temperature and centrifugal speed jointly affect the proportion of equiaxed grains and grain size. Combined with the analysis of grain size and its distribution characteristics, selecting the set of parameters with small grain size and more equiaxed grains is most conducive to the preparation of the ring with excellent performance and high material utilization. Therefore, the K417 superalloy ring was prepared with a pouring temperature of 1,380 °C and a centrifugal speed of 400 r·min^{-1} (P5 process).

3.2 Experiment results

3.2.1 Microstructure of K417 superalloy ring

The fine-grained K417 superalloy ring was obtained by centrifugal casting using optimized parameters. The microstructure of the ring is shown in Fig. 6. Figures 6(a) and (b) show the grain structure and porosity defects of the ring, respectively. Fine equiaxed grains are observed. The porosity defects are controlled below Grade one (standard 0.5%). Figures 6(c) and (d) exhibit the EBSD morphology and grain size statistics of the fine grain zone, respectively. The ring has an orientation-randomly equiaxial grain structure through inverse pole figure (IPF) map [Fig. 6(c)], and the average grain size is 67.48 μm [Fig. 6(d)]. The prepared K417 superalloy ring exhibits a fine grain structure (ASTM 4).

Figure 7 shows the morphology of the γ' phase in the K417 superalloy ring by centrifugal casting. The morphology of the γ' phase in the interdendritic regions is observed in Fig. 7(a), where the γ' phase appears as irregular, blocky particles with an average size of approximately 518 nm. The morphology of the γ' phase in the dendritic regions is observed in Fig. 7(b), which presents as regular, blocky shapes uniformly distributed throughout the as-cast microstructure, with an average size of about 441 nm.

Figure 8 shows the morphology of the precipitated phases and the EDS energy spectrum analysis of the K417 superalloy ring by centrifugal casting. The morphology and distribution of the precipitated phases are shown in Fig. 8(a). The matrix of K417 superalloy is composed of γ phase. The γ/γ' eutectic phase exhibits a sunflower-like structure with an overall size of about 65 μm. Carbides predominantly exist in two forms: strip-like or blocky, with significant size differences, averaging about 5–6 μm in size. Both the γ/γ' eutectic phases and carbides precipitate along the grain boundaries. EDS spectrum for γ/γ' eutectic phases and carbides are shown in Figs. 8(b) and (c), respectively. Figure 8(b) indicates that the γ/γ' eutectic phases are enriched with elements such as Al and Ti, which are known to form the γ' phase. Figure 8(c) shows that the carbides are typical MC carbides containing a high amount of Ti and Mo elements.

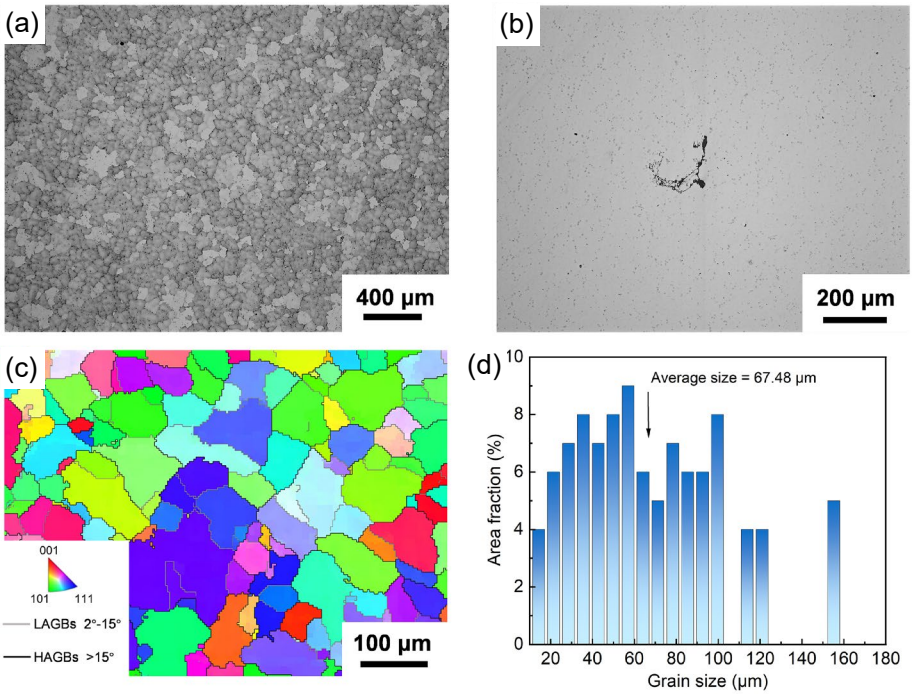


Fig. 6: Microstructure of K417 superalloy ring by centrifugal casting: (a) grain structure of the ring; (b) porosity defect of the ring; (c) inverse pole figure (IPF) map; (d) statistics of grain size

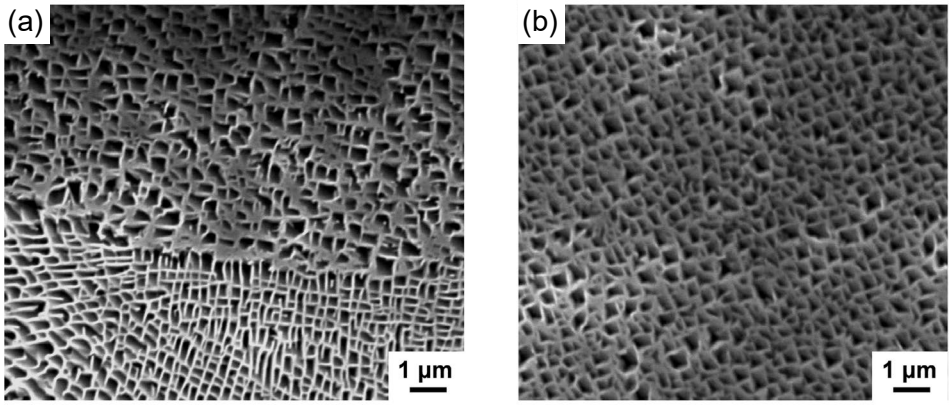


Fig. 7: Morphology of γ' phase in K417 superalloy ring by centrifugal casting: (a) in interdendrite; (b) in dendrite

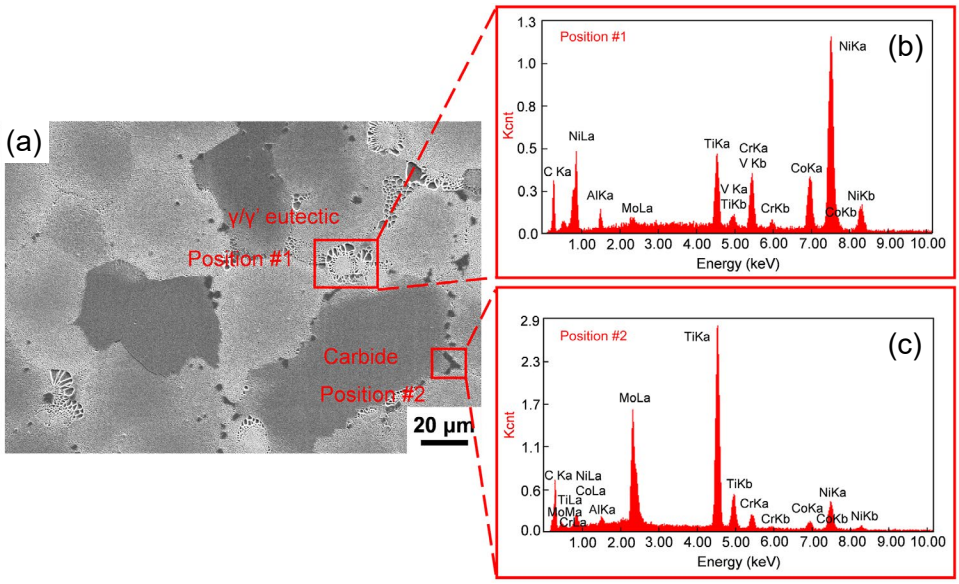


Fig. 8: Precipitated phases of K417 superalloy ring by centrifugal casting: (a) morphology and distribution of precipitated phases; (b) EDS energy spectrum of γ/γ' eutectic phase; (c) EDS energy spectrum of carbide

The radial distribution of K417 superalloy elements (Al, Ti, Mo, Cr, Co) in the ring was studied, as shown in Fig. 9. Figure 9(a) shows the content distribution of Al, Ti, and Mo elements from the outer ring to the inner ring, along the radial direction of the ring, and Fig. 9(b) exhibits the content distribution of Cr and Co elements along the same direction. The results exhibit that the content of Al, Ti, and Mo elements involved in the formation of precipitated phases fluctuates greatly at different positions, in contrast, the content of Cr and Co elements uniformly dissolved in the matrix changes more smoothly. There is no significant segregation in the whole, which indicates that the elements of the K417 superalloy ring obtained by centrifugal casting is evenly distributed and its quality is excellent.

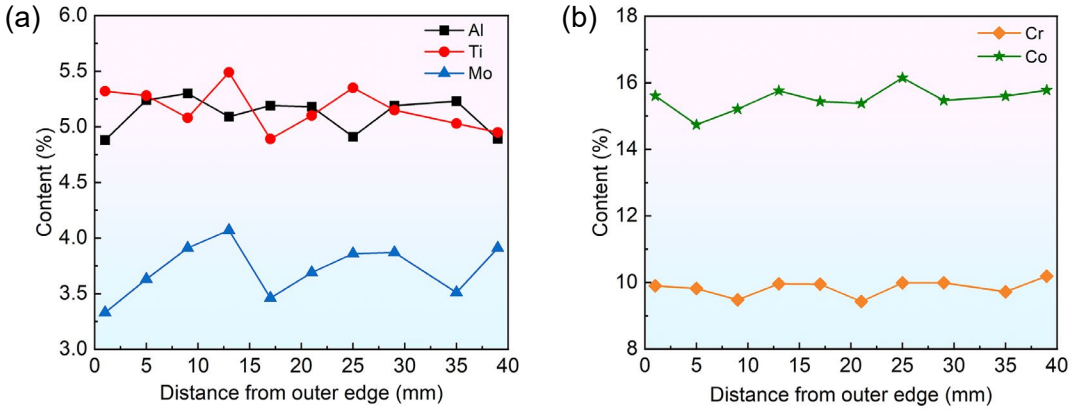


Fig. 9: Radial distribution of major alloy elements in K417 superalloy ring by centrifugal casting: (a) Al, Ti, Mo; (b) Cr, Co

3.2.2 Mechanical properties of K417 superalloy ring

Tensile tests were carried out at different testing temperatures, and the results are shown in Fig. 10 and Table 3. The tensile strength of the K417 superalloy ring at 20 °C is as high as 1,115.3 MPa, the yield strength is 908.9 MPa, and the elongation is 10.4%. At 900 °C, the tensile strength obviously decreases to 725 MPa, the yield strength decreases to 579.3 MPa, and the elongation is 8.5%. At 1,000 °C, the tensile strength further decreases to 409.6 MPa, the yield strength reduces to 335.3 MPa, and the elongation slightly increases to 9.1%. In general, with the increase of tensile temperature, the tensile strength and yield strength decrease obviously, and the plasticity decreases slightly.

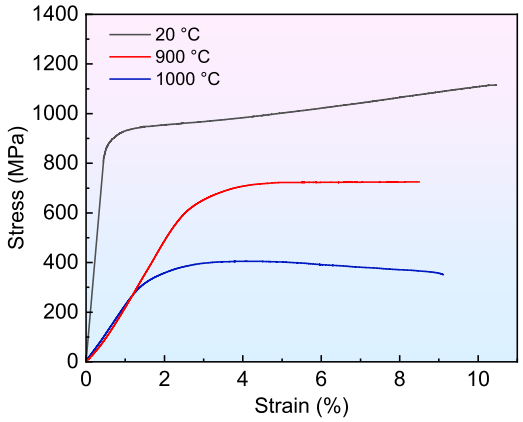


Fig. 10: Tensile curves of K417 superalloy ring by centrifugal casting under different testing temperatures

Table 3: Tensile properties of K417 superalloy ring by centrifugal casting

Testing temperature (°C)	Yield stress (MPa)	Tensile stress (MPa)	Elongation (%)
20	908.9	1,115.3	10.4
900	579.3	725.0	8.5
1,000	335.3	409.6	9.1

3.2.3 Tensile fracture and crack of K417 superalloy ring

In order to study the fracture formation mechanism of the K417 superalloy ring, the fractures were observed by SEM. Figure 10 indicates the tensile fracture morphology of K417 superalloy ring by centrifugal casting at different temperatures. Figures 11(a–c), (d–f), and (g–i) show the macroscopic and microscopic morphologies of the tensile fractures of the K417 superalloy at 20 °C, 900 °C and 1,000 °C, respectively. In Figs. 11(a–c), it can be seen that there are tearing edges, quasi-cleavage planes, and smaller dimples in tensile fracture at 20 °C. Precipitated phases and small cracks are observed in some micropores on the fracture surface, and the precipitated phase is determined as MC carbides rich in Ti and Mo by EDS [Fig. 11(c)]. The stress concentration at the carbides leads to the cracking of carbides, causing the failure of the matrix. The number of carbides in the micropores of the tensile fracture at 900 °C obviously increases, and the micropores become larger [Figs. 11(d–f)]. In many micropores, carbides are about to fall off from the matrix, which reduces the plasticity. The fracture surface exhibits distinct shear ridges, which are relatively numerous, with a few dimples present near the shear ridges. Fracture surface shows many pits caused by the shedding of precipitated phase and large cracks at 1,000 °C in Figs. 11(g–i). In general, the fracture surfaces at all the three temperatures clearly show micropores, indicating a micropore aggregation type of fracture. The fracture mechanism is a mixed ductile and brittle.

To explore the crack origin of tensile fractures, the longitudinal sections near the tensile fracture surfaces were observed by SEM, as shown in Fig. 12. Figures 12(a, b), (c, d), and (e, f) represent the longitudinal sections near the tensile fracture surfaces of the K417 superalloy at 20 °C, 900 °C, and 1,000 °C, respectively. Figures 12(a) and (b) show that the crack near the tensile fracture at 20 °C originates from the eutectic phases and the breakage and shedding of carbides. The connection between γ/γ' eutectic phases and matrix is weak, and cracks are easy to occur [Fig. 12(a)]. Figure 12(c) indicates that the fine crack sources near the tensile fracture surface mainly originate from carbides at 900 °C, where the connection between carbides and the matrix at grain boundaries is weak. Along the marked route in Fig. 12(c), microcracks expand into larger cracks that extend to the surface. Figures 12(c) and (d) show that the fracture of tensile fracture surface at 900 °C is a mixed intergranular and transgranular fracture, while the crack propagation of tensile fracture surface at 1,000 °C is primarily intergranular fracture [Figs. 12(e) and (f)].

3.2.4 Deformation microstructure of K417 superalloy after tensile tests

To further study the dislocation characteristics after tensile deformation at different tensile testing temperatures, the EBSD morphology of the longitudinal section of the tensile fracture at different temperatures was observed, as shown in Fig. 13. Figures 13(a–c) show the KAM (Kernel average misorientation) maps of the longitudinal sections near the tensile fracture surfaces at 20 °C, 900 °C, and 1,000 °C, respectively, where blue and red colors represent the lowest and highest dislocation densities, respectively. All tensile samples exhibit higher stress concentrations at the boundaries after deformation, which can be attributed to the presence of fine carbides at the grain boundaries. Figure 13(a) shows that in addition to the higher dislocation density at the grain boundaries, there are also many dislocations within the grains in tensile samples at 20 °C, with general stress concentration at the grain boundaries and a more dispersed stress distribution within the grains. The KAM map at 20 °C shows a wider region of orientation difference. The results in Figs. 13(b) and (c) show that the misorientation region becomes narrower due to the increase of tensile temperature. According to the KAM maps, the KAM values at the fracture longitudinal sections

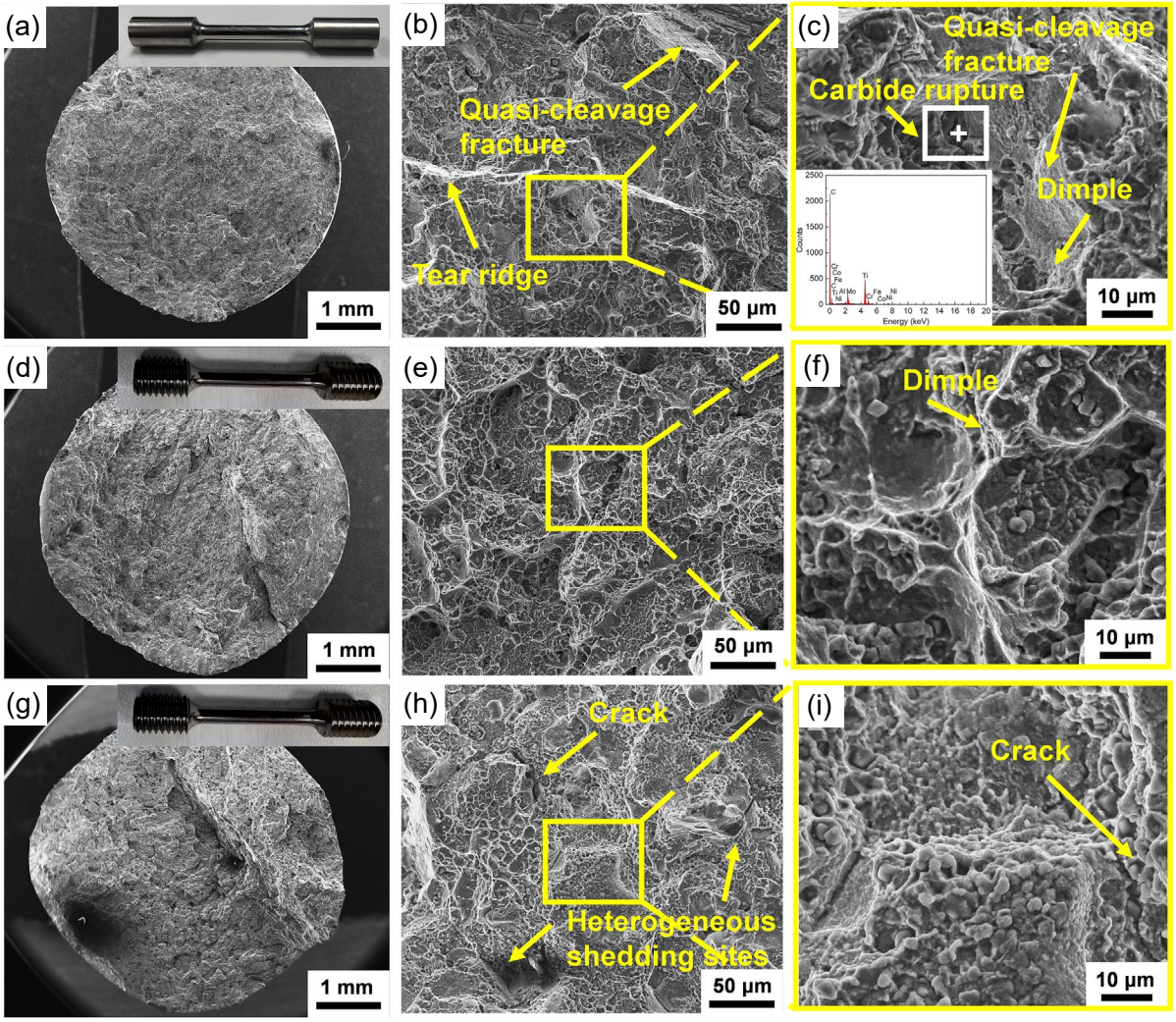


Fig. 11: Tensile fracture morphology of K417 superalloy ring by centrifugal casting at different temperatures: (a–c) 20 °C; (d–f) 900 °C; (g–i) 1,000 °C

at 20 °C, 900 °C, and 1,000 °C are 0.52°, 0.39°, and 0.40°, respectively, and the dislocation density decreases with the increase of tensile temperature.

Additionally, Figs. 13(d–f) are the IPF maps of the longitudinal sections near the tensile fracture surfaces at 20 °C, 900 °C, and 1,000 °C, respectively. According to the IPF maps, the grain sizes at the tensile fractures at different testing temperatures are observed. The average grain sizes near the tensile fractures at 20 °C, 900 °C, and 1,000 °C are approximately 78.79 μm, 106.83 μm, and 108.59 μm, respectively. The grain sizes of the fractures are relatively uniform and small at 20 °C. With the increase of tensile temperature, the grains near the tensile fractures at 900 °C and 1,000 °C exhibit coarsening, and the distribution of grain sizes becomes non-uniform.

4 Discussion

4.1 Microstructure optimization analysis of K417 superalloy

With the increase of centrifugal speed, the average grain size is distributed around 207 μm in Fig. 5. The centrifugal speed has a multifaceted effect on grain growth. Primarily, it influences the flow of the melt. On the one hand, it can cause melt turbulence and stir the melt to break the dendrites. On the other hand, it also leads to a situation where solute at the solidification front is less likely to accumulate, failing to meet the compositional undercooling required for the formation of equiaxed grains[29]. Moreover, the centrifugal speed has an inconspicuous effect on heat dissipation, hence, its impact on the average grain size is not straightforward. According to the simulation results presented in Fig. 5, it is observed that as the pouring temperature increases from 1,380 °C to 1,540 °C, the average grain size also increases. This is attributed to the fact that a higher pouring temperature results in a longer solidification time for the melt, allowing both equiaxed and columnar grains more time to grow[30]. Furthermore, excessively high pouring temperatures can cause the already solidified parts to remelt, reducing the number of nucleation sites and grains, thereby increasing the average grain size[31]. Conversely, a lower pouring temperature is conducive to the survival of grains that detach from the crystallization front, and a lower superheat generates more free particles, which favors the growth of equiaxed grains and increases the volume

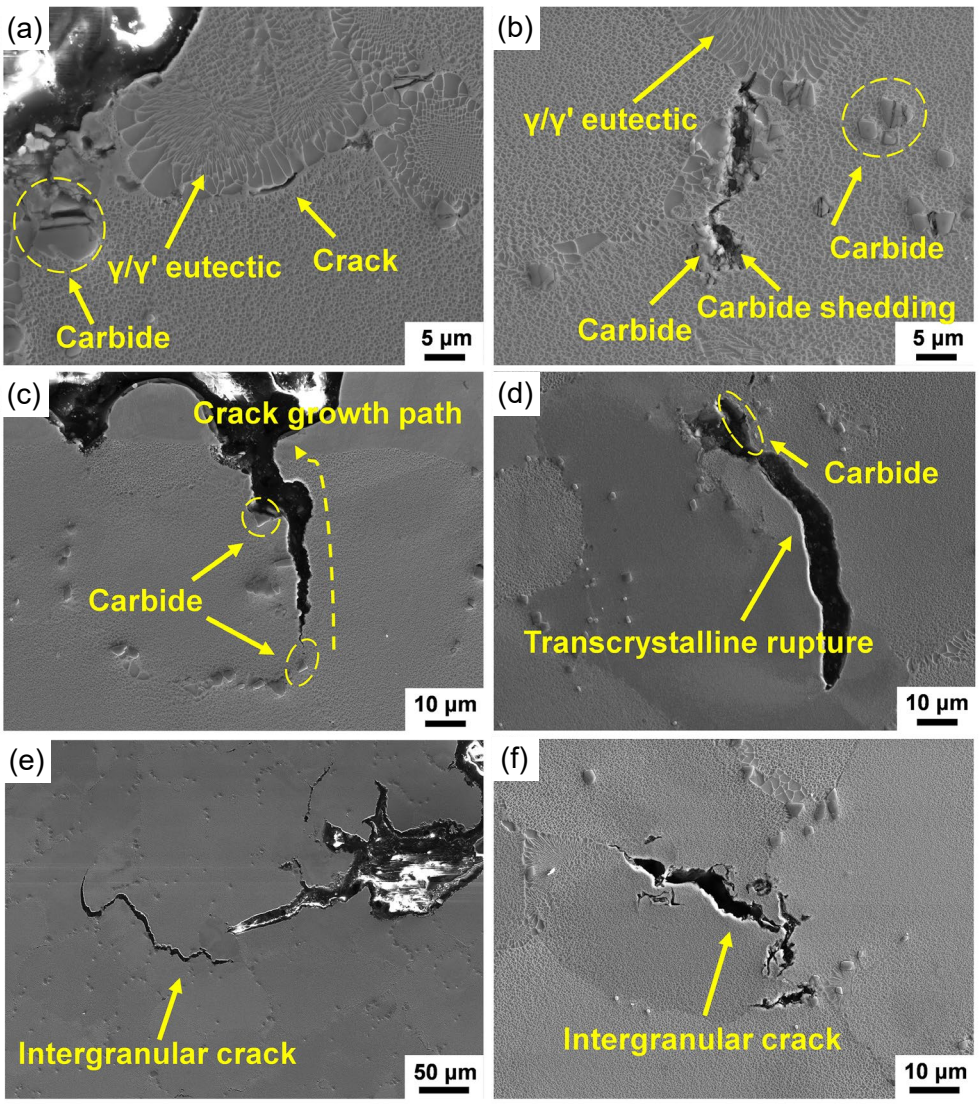


Fig. 12: Longitudinal section morphology of tensile fractures: (a, b) cracks near the tensile fracture at 20 °C; (c, d) cracks near the tensile fracture at 900 °C; (e, f) cracks near the tensile fracture at 1,000 °C

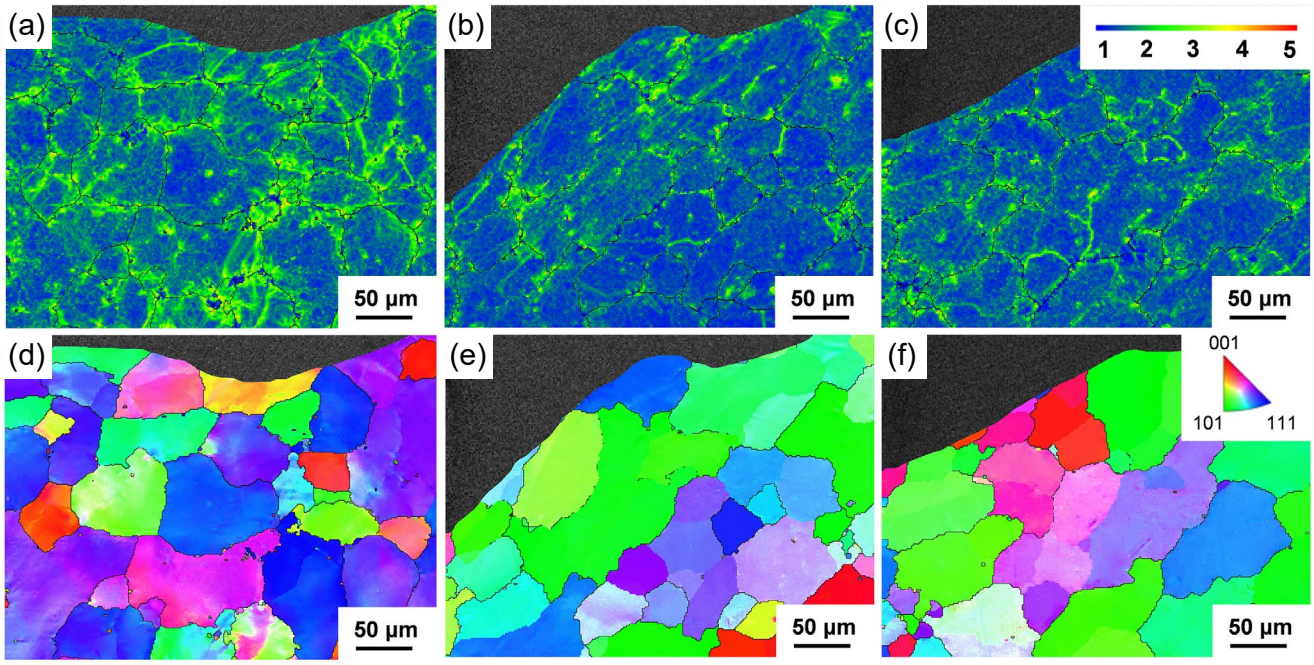


Fig. 13: EBSD morphology of longitudinal section of tensile fractures at 20 °C (a, d), 900 °C (b, e), and 1,000 °C (c, f)

fraction of the equiaxed grain region[28]. Therefore, when the pouring temperature is 1,380 °C, the volume fraction of the equiaxed grain region is the highest.

The prepared K417 ring exhibits a fine grain structure (ASTM 4), as shown in Figs. 6(a, c, d). The main reasons are as follows. Firstly, the formation of grains in the centrifugal casting involves a complex crystallization and growth process. A large number of alloy elements and impurities that appear in the solidification stage of the K417 superalloy melt can lead to heterogeneous nucleation and grain growth. The rate of heterogeneous nucleation is calculated using Eq. (1)[28, 32]:

$$I = f_1 N_L \exp\left[-B \cdot \frac{f(\theta)}{\Delta T^2}\right] \quad (1)$$

where ΔT represents the degree of undercooling. An increase in undercooling leads to an increased nucleation rate and a decrease in grain size. During the actual centrifugal casting, the K417 superalloy melt comes into contact with the mold, creating a significant temperature difference almost instantaneously, resulting in a high degree of undercooling for the alloy liquid and thus a smaller average grain size[33]. Additionally, when the K417 superalloy melt contacts the mold wall during filling, it undergoes rapid cooling, which can prevent excessive grain growth. Rapid cooling allows nucleation to occur quickly and helps maintain a small grain size before solidification[34]. Additionally, at the moment when the molten metal is poured into the mold, a layer of fine-grained chill zone is immediately formed at the mold wall due to its chilling effect. The melt influenced by rapidly centrifugal casting creates intense melt turbulence at the solid-liquid interface ahead of the solidification front, where dendrites nucleated earlier on the mold wall are continuously eroded, leading to dendrite fragmentation and grain shedding. The shed, free-floating grains enter into the new melt, resulting in grain multiplication[35, 36]. This is considered the primary reason for the refinement of the solidification microstructure in the centrifugal casting[37].

The assessment of porosity defects of the K417 superalloy ring shows that the overall porosity defects are controlled below Grade one, and the microstructure is dense, as shown in Fig. 6(b). The reasons for the formation of porosity defects in centrifugal casting process are complex, among which the fundamental reason is that the molten metal can no longer supply the volume loss during the shrinkage process to the mushy zone[38]. After the well-developed coarse dendrites in the solidification zone interconnect to form a dendritic skeleton, the unsolidified molten metal is divided into a molten pool that does not communicate with each other, forming porosity defects in the cast. In addition, the formation of porosity is closely related to the temperature gradient and cooling rate at the solidification front. According to the Niyama criterion, as shown in Eq. (2), when the temperature gradient and cooling rate of a casting satisfy the Niyama criterion, porosity will form[39, 40].

$$\frac{C_L}{R} < C_1, \quad \frac{C_L}{\sqrt{C_L R}} < C_2 \quad (2)$$

In Eq. (2), C_L is the temperature gradient of the solidification front; R is the solidification rate; C_1 and C_2 are the critical criterion value of porosity; $C_L R$ is the cooling rate.

However, different from the traditional gravity casting, the K417 superalloy liquid is subjected to significant centrifugal force and filling pressure in the centrifugal casting, so it can effectively flush the previously solidified parts during the pouring process, leading to good feeding and high microstructural density. Moreover, as mentioned above, the K417 superalloy melt contacts the mold wall, forming a large temperature gradient and a narrow solidification zone, which results in good feeding of the molten metal. The rapid cooling of the molten metal within a certain range can also cause the melt to cool and solidify quickly within the mold, thereby reducing the generation and expansion of bubbles in the melt, and controlling porosity defects[41]. Additionally, the K417 superalloy ring was fabricated using vacuum centrifugal casting, and the vacuum condition can reduce the mixing of impurity gases from the air into the alloy melt. Besides, the filling and solidification under vacuum condition are also conducive to the expulsion of gases from the casting, greatly avoiding the occurrence of porosity, thus resulting in a denser microstructure in the ring prepared by this process.

4.2 Crack propagation and fracture formation mechanism of K417 superalloy during tensile deformation

The tensile fracture of K417 superalloy involves the evolution of stress states at multiphase interfaces and the synergistic effect with crack propagation[42]. At 20 °C, the fracture process is primarily controlled by the competition between local stress concentration effects and interface strengths. Due to the semi-coherent relationship of {111}MC || {111}γ/γ' and <011>MC || <011>γ/γ', there is a high density of mismatch dislocations at the interfaces. Under tensile loading, these interface dislocations are easily activated, leading to local stress concentration[42]. When the applied load reaches a critical value, initial cracks preferentially nucleate at the interfaces between eutectic phases and the matrix, as well as between carbides and the matrix. Figure 12(a) shows that the tensile crack nucleates at the interface of γ/γ' eutectic and the matrix under the continuous action of load, expanding to form a typical “zigzag” fracture path at 20 °C. Figure 12(b) shows that the crack originates from the breaking of MC carbides. It has been shown that MC carbides generally precipitate from the residual liquid between dendrites after the crystallization of matrix, and since MC carbides have a uniform nucleation pattern and their crystal orientations are different from that of the matrix, they often serve as crack initiation sites leading to matrix failure[42-44].

When the temperature is raised to 900 °C, a significant change in the fracture mechanism occurs. The fracture mechanism is the coupled effect of thermal stress and applied stress. In Fig. 12(c), the crack initiates from fine carbides and gradually propagates along the grain boundaries to the fracture surface. Due to the different coefficients of thermal expansion between MC carbides and the matrix, crack propagation is

more likely to occur at the interfaces connecting them with the matrix, especially at the carbide corners, where the geometric effect amplifies stress concentration, making it a preferred site for crack initiation[45, 46]. As the temperature increases, both intergranular and intragranular strengths are reduced to varying degrees, but the rate of decrease in intergranular strength is faster. At 900 °C, the grain boundaries still maintain a certain level of strength, hence in Fig. 12(d), it is evident that the crack traverses the grain boundaries and extends into the grains. Tensile testing at 900 °C results in a unique "transgranular-intergranular" mixed fracture mode.

Upon further heating to 1,000 °C, the fracture mode completely transforms to grain boundary dominated failure. Figures 12(e) and (f) clearly show the crack propagation along grain boundaries, primarily due to the significant weakening of grain boundary strength at high temperatures. Simultaneously, grain boundary sliding becomes exceptionally active, particularly at the triple points of grain boundaries where the stress concentration effect is most pronounced, making it the preferred site for crack initiation[47].

4.3 Microstructure of K417 superalloy during tensile deformation

The K417 superalloy ring exhibits a fine grain size, with the strengthening γ' phase measuring between 400–600 nm. The fine strengthening γ' phase plays a major role in pinning the dislocation movement, which directly leads to the excellent tensile properties of the ring at 20 °C, making the tensile strength up to 1,115.3 MPa, as shown in Fig. 10 and Table 3. With increasing the tensile temperature, the results from the tensile fracture KAM map in Fig. 13 show that dislocation slip increases and dislocation density decreases at high temperatures. High temperatures lead to an increase in atomic diffusion rates and increased dislocation activity, weakening the pinning effect on dislocations, shifting the mechanism from shearing the γ' phase to bypassing the γ' phase, which reduces the alloy's strength[48]. Typically, as the tensile temperatures increase, the slip and interaction of dislocations are also enhanced, and the aggregation and movement of dislocations reduce the dislocation density, further reducing the strength of the material[49]. The results from the IPF maps of the fracture in Fig. 13 show that the grain size of the tensile fracture at high-temperature appears to be non-uniform, which causes the incompatible deformation. This is also one of the reasons for the reduction in tensile strength. Moreover, as the tensile temperatures increase, the average grain size of the fracture increases, leading to the decrease of strength. With the increase of tensile temperatures, the plasticity of the K417 superalloy ring is slightly reduced. This may be due to intermediate temperature brittleness, which is generally caused by the promotion of grain boundary segregation with temperatures increasing, and this phenomenon is common in nickel-based superalloys[45, 50-52]. Additionally, tensile at 900 °C and 1,000 °C can lead to the weakening of grain boundaries, reducing the resistance to crack propagation, thereby leading to a reduction in the final deformation before fracture[47]. In general, the higher strength of the K417 superalloy is primarily attributed to the uniform distribution of the strengthening phase γ' within the matrix, which pins dislocations and hinders dislocations to move. The γ' phase and the γ matrix phase act concurrently to enhance the strength of the alloy[53].

5 Conclusions

The K417 superalloy ring is mainly used in hot end components such as aerospace engine combustion chamber. In order to realize the preparation of high-quality rings with short process and low cost, in this study, the optimal centrifugal casting process parameters were obtained by ProCAST firstly, and then the K417 superalloy ring with equiaxed fine grains, dense structures, uniform composition and excellent mechanical properties was successfully fabricated by vacuum centrifugal casting. The results can be concluded as follows:

(1) According to the comparison of multiple sets of simulation results, the effect of pouring temperature on the average grain size is much more obvious than that of centrifugal rotation speed. The pouring temperature in actual centrifugal casting is determined to be 1,380 °C and the rotational speed is 400 $r \cdot min^{-1}$.

(2) The prepared K417 ring exhibits a fine grain structure (ASTM 4). The γ' phase is uniformly distributed in the matrix as the main strengthening phase, accompanied by γ/γ' eutectic phases and MC carbides precipitated at the grain boundaries. The porosity defects of the K417 superalloy ring are overall controlled below Grade one. The elemental distribution shows excellent uniformity of the ring.

(3) The tensile strength of the K417 superalloy ring is 1,115.3 MPa at 20 °C, 725 MPa at 900 °C, and 409.6 MPa at 1,000 °C, with the elongation of 10.4%, 8.5%, and 9.1%, respectively. With the increase of tensile temperature, the tensile strength and yield strength decrease significantly, and the plasticity decreases slightly.

(4) MC carbides and γ/γ' eutectic phases are found to be the main crack sources at the tensile fractures of the centrifugal cast ring. As the tensile temperature increases, the fracture form gradually transforms from transgranular-intergranular fracture at 900 °C to intergranular fracture at 1,000 °C. The dislocation density decreases with the increase of tensile temperature. In general, the reason for the higher strength of the K417 superalloy is the uniform distribution and its fine grain size of the γ' strengthening phase in the matrix.

Acknowledgments

This work was financially supported by the Natural Science Foundation of China (No. 52071065), the Fundamental Research Funds for the Central Universities (No. N2007007), the National Key R&D Program of China (No. 2016YFB-0301201), the Startup Research Fund of Henan Academy of Sciences (No. 242017003), and the Joint Fund of Henan Province Science and Technology R&D Program (No. 225200810040).

Conflict of interest

The authors declare that they have no competing financial interests or personal relationships that could have appeared to influence the work in this paper.

References

[1] Li J P, Zhang H R, Gao M, et al. Effect of vacuum level on the interfacial reactions between K417 superalloy and Y_2O_3 crucibles. Vacuum, 2020, 182: 109701.
[2] Jangali S G, Gaitonde V N, Kulkarni V N, et al. Analyzing the effect of cutting parameters on forces and tool-tip temperature in turning of nickel-based superalloy using FE simulation. Materials Today: Proceedings, 2022, 49: 1833–1843.
[3] Bian W D, Zhang H R, Zhang X L, et al. Comprehensive influence of Y on K417 superalloy: Purification, interactions among the alloy elements and high temperature properties. Materials Science and Engineering: A, 2019, 755: 190–200.
[4] Hu Y, Liu D, Yang Y, et al. Multi-objective optimization of cavity design for GH4738 superalloy profile ring rolling process based on FEM and RSM. The International Journal of Advanced Manufacturing Technology, 2022, 123(7–8): 2929–2940.
[5] Lu K L, Zhao G Y, Guo Z H, et al. Review on multi-pass rolling forming of thin-walled ring with complex section. Journal of Physics: Conference Series, 2024, 2706(1): 012033.
[6] Qin F C, Li Y T, Qi H O, et al. Microstructure-texture-mechanical properties in hot rolling of a centrifugal casting ring blank. Journal of Materials Engineering and Performance, 2016, 25(3): 1237–1248.
[7] Zeng G, Liu C M, Gao Y H, et al. Microstructure and mechanical properties of AZ80-Ag alloy processed by hot ring rolling. Materials Science and Engineering: A, 2016, 674: 491–497.
[8] Hu Y, Liu D, Zhu X L, et al. Effect of rolling passes on thermal parameters and microstructure evolution via ring-rolling process of GH4738 superalloy. The International Journal of Advanced Manufacturing Technology, 2018, 96(1–4): 1165–1174.
[9] Zayadi H, Parvizi A, Farahmand H R, et al. Investigation of cavity filling in profile ring rolling process for T-shape ring. Proceedings of the Institution of Mechanical Engineers, Part L: Journal of Materials: Design and Applications, 2021, 235(11): 2505–2515.
[10] Zhu X L, Dong E T, Qiao X M, et al. Evaluation methods and coupled optimization at macro- and micro-scales for profiled ring rolling of Inconel718 alloy. Materials, 2024, 17(18): 4538.
[11] Yang Y J, Wang X Y, Li X M, et al. Numerical simulation on solidification during vertical centrifugal casting process for TC4 alloy wheel hub with enhanced mechanical properties. Materials, 2023, 17(1): 184.
[12] Wang D C, Liao M L, Wang Y, et al. Optimization of centrifugal casting process parameters by Taguchi method to reduce shrinkage porosity ratio of K417 superalloy. Modern Physics Letters: B, 2022, 36(30n31): 2250164.
[13] Liu L B, Hu C H, Zhang Y H, et al. Melt flow, solidification structures, and defects in 316 L steel strips produced by vertical centrifugal casting. Advances in Manufacturing, 2023, 11(4): 636–646.
[14] Barella S, Gruttadauria A, Mapelli C, et al. Solidification microstructure of centrifugally cast Inconel 625. China Foundry, 2017, 14(4): 304–312.
[15] Mallick A, Setti S G, and Sahu R K. Centrifugally cast functionally graded materials: Fabrication and challenges for probable automotive cylinder liner application. Ceramics International, 2023, 49(6): 8649–8682.
[16] Lv S K, Dou R F, Yu B, et al. Experimental and numerical studies on the influence of centrifugal casting parameters on the solidification structure of Al-Cu alloy. Materials Research Express, 2022, 9(10): 106506.
[17] Kim W, Jang K, Ji C, et al. Effects of heat treatment on the microstructure and hardness of A356 (AlSi7Mg0.3) manufactured by vertical centrifugal casting. Applied Sciences, 2021, 11(23): 11572.
[18] Yang Y H, Song B, Yang Z B, et al. The refining mechanism of super gravity on the solidification structure of Al-Cu alloys. Materials, 2016, 9(12): 1001.
[19] Li S Y, Qin S Y, Xi X J, et al. Solidified structure refinement of H13 tool steel under a multi-rotational speed super gravity field. Metals, 2020, 10(11): 1428.
[20] Liang H C, Kang J M, Zhao D Z, et al. Simulation and analysis of AZ80 magnesium alloy centrifugal casting. Journal of Physics: Conference Series, 2023, 2459(1): 012049.
[21] Li B, Bai W, Yang K, et al. Revealing the microstructural evolution and strengthening mechanism of Mg-5.5Gd-3Y-1Zn-0.5Mn alloy in centrifugal casting and subsequent hot rolling. Journal of Alloys and Compounds, 2024, 984: 173950.
[22] Wang X X, Chen R R, Wang Q, et al. Influence of casting temperature and mold preheating temperature on centrifugal casting by numerical simulation. Journal of Materials Engineering and Performance, 2023, 32(15): 6786–6809.
[23] Qin F C, Qi H P, Li Y T, et al. Relationship of grain size, texture distribution, and mechanical properties of 25Mn casting flange blank subjected to hot ring rolling. Journal of Materials Engineering and Performance, 2021, 30(2): 1128–1138.
[24] Ma Z D, Peng Q, Wei G B, et al. Improvement of microstructure, mechanical property and corrosion resistance of Mg-9Li-3Al-1Ca alloy through centrifugal casting. Metals and Materials International, 2021, 27(11): 4498–4509.
[25] Kang M D, Wang J, Gao H Y, et al. Study on the castability and mechanical properties of thin-walled nickel-base superalloy. Materials Science and Technology, 2017, 33(3): 326–332.
[26] Yang L, Chai L H, Liang Y F, et al. Numerical simulation and experimental verification of gravity and centrifugal investment casting low pressure turbine blades for high Nb-TiAl alloy. Intermetallics, 2015, 66: 149–155.
[27] Abdullin A D. New capabilities of the ProCAST 2017 software in simulating casting processes. Metallurgist, 2017, 61(5–6): 433–438.
[28] Xin M L, Wang Z D, Lu B, et al. Effects of different process parameters on microstructure evolution and mechanical properties of 2060 Al-Li alloy during vacuum centrifugal casting. Journal of Materials Research and Technology, 2022, 21: 54–68.
[29] Chang S R, Kim J M, and Hong C P. Numerical simulation of microstructure evolution of Al alloys in centrifugal casting. ISIJ International, 2001, 41(7): 738–747.
[30] Mohapatra S, Sarangi H, and Mohanty U K. Effect of processing factors on the characteristics of centrifugal casting. Manufacturing Review, 2020, 7(1): 26.
[31] Shi Z X, Liu S Z, Wang X G, et al. Effect of melting temperature on the microstructure stability of a Ni-based single crystal superalloy. Procedia Engineering, 2015, 99: 1415–1420.
[32] Kurz W and Fisher D J. Fundamentals of solidification: Fourth revised edition. Trans Tech Publications, 1998: 35.
[33] Li Y, Wang Y, Qin X M, et al. Ellipsoidal equiaxial grain of 7055 aluminium alloy in vacuum centrifugal casting. Materials Science and Technology, 2023, 39(3): 362–368.
[34] Shailesh R A, Tattimani M S, and Rao S S. Understanding melt flow behavior for Al-Si alloys processed through vertical centrifugal casting. Materials and Manufacturing Processes, 2015, 30(11): 1305–1311.

[35] Luo D, Wang H Y, Ouyang Z T, et al. Microstructure and mechanical properties of Mg-5Sn alloy fabricated by a centrifugal casting method. Materials Letters, 2014, 116: 108–111.
[36] Sui Y W, Li B S, Liu A H, et al. Evolution of solidification microstructure of centrifugal cast Ti-6Al-4V alloy. Materials Science and Technology, 2009, 25(12): 1458–1461.
[37] You F J, Zhao X B, Yue Q Z, et al. A review on solidification of alloys under hypergravity. Progress in Natural Science: Materials International, 2023, 33(3): 279–294.
[38] Esser P, Schankies C, Khalajzadeh V, et al. Advanced modeling of shrinkage porosity in castings. IOP Conference Series: Materials Science and Engineering, 2020, 861(1): 012022.
[39] Ivanina E S, Monastyrskiy V P, and Ershov M Y. Quantitative estimation of formation of shrinkage porosity by the Niyama criterion. Inorganic Materials: Applied Research, 2022, 13(1): 100–105.
[40] Bhoraniya D, Dharaiya V, and Sata A. Application of Niyama criterion to predict shrinkage porosity in vertical centrifugal casting of ASTM A356 alloy. International Journal of Process Management and Benchmarking, 2022, 12(3): 395.
[41] Mahomed N. Shrinkage porosity in steel sand castings: Formation, classification and inspection. In: Casting Processes and Modelling of Metallic Materials. Intech Open, 2021.
[42] Wang F, Xu W L, Ma D X, et al. Co-growing mechanism of γ/γ′ eutectic on MC-type carbide in Ni-based single crystal superalloys. Journal of Alloys and Compounds, 2019, 792: 505–509.
[43] Wang F, Ma D X, and Bührig-Polaczek A. Eutectic formation during solidification of Ni-based single-crystal superalloys with additional carbon. Metallurgical and Materials Transactions: A, 2017, 48(11): 5442–5448.
[44] Gui W M, Zhang X T, Zhang H Y, et al. Melting of primary carbides in a cobalt-base superalloy. Journal of Alloys and Compounds, 2019, 787: 152–157.
[45] Du B N, Hu Z Y, Sheng L Y, et al. Tensile, creep behavior and microstructure evolution of an as-cast Ni-based K417G polycrystalline superalloy. Journal of Materials Science & Technology, 2018, 34(10): 1805–1816.
[46] Yang C X, Xu Y L, Zhang Z X, et al. Improvement of stress-rupture life of GTD-111 by second solution heat treatment. Materials & Design, 2013, 45: 308–315.
[47] Du B N, Yang J X, Cui C Y, et al. Effects of grain refinement on the microstructure and tensile behavior of K417G superalloy. Materials Science and Engineering: A, 2015, 623: 59–67.
[48] Peng T, Wang Y L, Yang B, et al. Tensile properties and deformation mechanisms of nimonic 105 superalloy at different temperatures. Materials Science and Engineering: A, 2021, 828: 142028.
[49] Wan Z P, Hu L X, Sun Y, et al. Effect of solution treatment on microstructure and tensile properties of a U720Li Ni-based superalloy. Vacuum, 2018, 156: 248–255.
[50] Zheng L, Schmitz G, Meng Y, et al. Mechanism of intermediate temperature embrittlement of Ni and Ni-based superalloys. Critical Reviews in Solid State and Materials Sciences, 2012, 37(3): 181–214.
[51] Sheng L Y, Yang F, Xi T F, et al. Microstructure and room temperature mechanical properties of NiAl-Cr(Mo)-(Hf, Dy) hypoeutectic alloy prepared by injection casting. Transactions of Nonferrous Metals Society of China, 2013, 23(4): 983–990.
[52] Zheng L, Chellali R, Schlesiger R, et al. Intermediate temperature embrittlement in high-purity Ni and binary Ni(Bi) alloy. Scripta Materialia, 2011, 65(5): 428–431.
[53] Xia W S, Zhao X B, Yue L, et al. Microstructural evolution and creep mechanisms in Ni-based single crystal superalloys: A review. Journal of Alloys and Compounds, 2020, 819: 152954.